

# The Effect of General Strain on the Band Structure and Electron Mobility of Silicon

Enzo Ungersboeck, Siddhartha Dhar, *Student Member, IEEE*, Gerhard Karlowatz, Viktor Sverdlov, Hans Kosina, *Member, IEEE*, and Siegfried Selberherr, *Fellow, IEEE*

**Abstract**—A model capturing the effect of general strain on the electron effective masses and band-edge energies of the lowest conduction band of silicon is developed. Analytical expressions for the effective mass change induced by shear strain and valley shifts/splittings are derived using a degenerate  $k \cdot p$  theory at the zone-boundary  $X$  point. Good agreement to numerical band-structure calculations using the nonlocal empirical pseudopotential method with spin-orbit interactions is observed. The model is validated by calculating the bulk electron mobility under general strain with a Monte Carlo technique using the full-band structure and the proposed analytical model for the band structure. Finally, the impact of strain on the inversion-layer mobility of electrons is discussed.

**Index Terms**—Band structure, MOS devices, shear strain, strain/stress, strained-silicon (Si), surface mobility.

## I. INTRODUCTION

**S**TARTING with the 90-nm CMOS technology node, strain engineering takes a key position among other technological innovations since it is cost effective and the beneficial effect of strain on the device performance is comparatively large. Ever since, increasing emphasis is put on strain technologies to further enhance chip performance in upcoming CMOS technology nodes.

The influence of strain on the mobility of intrinsic silicon (Si) was first investigated in the early 1950s [1], [2]. While strain effects were not exploited initially, strained-Si was revived at Massachusetts Institute of Technology in the early 1990s [3]. In 1992, it was first demonstrated that n-channel MOSFETs with a strained-Si channel exhibit a 70% higher effective mobility  $\mu_{\text{eff}}$  than those with unstrained Si [4], [5]. Since that time, semiconductor industry has adopted several different technologies to introduce strain in the Si channel of MOSFETs.

The linear piezoresistance coefficients of Si provide a simple method to estimate the effect of strain on the mobility of intrinsic Si. However, two problems arise when using models based on the piezoresistance coefficients of bulk Si: 1) In scaled devices, the strong quantum confinement has to be taken into account; thus, the bulk piezoresistance coefficients cannot be used to calculate the channel mobility. 2) The saturation of

Manuscript received January 3, 2007; revised May 8, 2007. The review of this paper was arranged by Editor S. Takagi.

The authors are with the Institut für Mikroelektronik, Technische Universität Wien, 1040 Vienna, Austria (e-mail: ungersboeck@iue.tuwien.ac.at).

Color versions of one or more of the figures in this paper are available online at <http://ieeexplore.ieee.org>.

Digital Object Identifier 10.1109/TED.2007.902880

mobility enhancement at large strain cannot satisfactorily be modeled using piezoresistance coefficients. A much better understanding can be obtained when taking into account the effect of strain on band structure and solving the Boltzmann transport equation using a Monte Carlo (MC) algorithm [6]–[8]. However, up to now, most theoretical work has been performed for biaxially strained-Si, whereas a thorough theoretical analysis of electron mobility enhancement in arbitrarily strained-Si is missing. This fact is surprising because in the state-of-the-art CMOS technologies, strain can be induced in the transistor channel via various stressors and/or from the virtual substrate, and the resulting strain is neither purely biaxial nor uniaxial.

In this paper, the effect of a general strain tensor on the band structure and the bulk and channel mobilities of electrons is investigated. The band-structure calculation of strained-Si is described in Section II. Special focus is put on the effect of shear strain as it induces a large effective mass change for electrons. In Section III, we describe the effect of strain on the mobility enhancement in bulk Si and in Si inversion layers with one and two interfaces.

## II. BAND-STRUCTURE MODELING

The empirical pseudopotential method (EPM) [9], including nonlocal effects and spin-orbit coupling, is frequently used to calculate the band structure of semiconductors, as this method is efficient and requires only a small number of parameters. These parameters are usually calibrated to match energy gaps and effective masses determined from experiments and are available for a large set of materials [10]. The method can be very naturally adapted to incorporate strain effects and has been used to investigate the band structure of biaxially strained-Si<sub>1-y</sub>Ge<sub>y</sub> grown on Si<sub>1-x</sub>Ge<sub>x</sub> for various surface orientations [6], [11], [12]. Since local process-induced strain in today's strain technologies is generally not biaxial, in this paper, we have shown how general strain conditions can be incorporated into the band-structure calculation. Special focus is put on the orthorhombic distortion of the crystal resulting from uniaxial stress along the [110] direction, since this type of strain is frequently used to enhance the electron mobility in n-channel MOSFETs.

For band-structure calculations, we followed the work of Rieger and Vogl [12]. In Table I, the parameters employed in the EPM calculations are listed. They consist of the three local form factors  $V_{\sqrt{3}}$ ,  $V_{\sqrt{8}}$ , and  $V_{\sqrt{11}}$ , the two parameters

TABLE I  
PARAMETERS EMPLOYED IN THE BAND-STRUCTURE CALCULATION OF Si

EPM parameters	Si value	Mat. parameters	Si value
$V_{\sqrt{3}}$ (Ry)	-0.2241	$a_0$ (Å)	5.43
$V_{\sqrt{8}}$ (Ry)	0.052	$c_{11}$ (GPa)	167.5
$V_{\sqrt{11}}$ (Ry)	0.0724	$c_{12}$ (GPa)	65.0
$A_0$ (Ry)	0.03	$c_{44}$ (GPa)	79.6
$R_0$ (Å)	1.06	$\xi$	0.53
$\mu$ (Ry)	0.00023		
$\zeta$ (Å <sup>-1</sup> )	7.5589		

$A_0$  and  $R_0$  to model the nonlocal correction, and the two parameters  $\mu$  and  $\zeta$  entering the spin-orbit interaction term. The parameters are essentially equal with the parameter set provided in [12], with the exception of  $\mu$  and  $\zeta$ , which have been adjusted to yield the desired split-off energy of 44 meV in the unstrained lattice.

### A. EPM Including General Strain Tensor

To handle arbitrary strain conditions, four modifications in the band-structure calculation are implied.

- 1) The direct lattice vectors  $\mathbf{a}'_i$  of the strained crystal have to be calculated by deforming the vectors  $\mathbf{a}_i$  of the unstrained crystal, i.e.,

$$\mathbf{a}'_i = \mathbf{a}_i + \sum_j \varepsilon_{ij} \mathbf{a}_j \quad (1)$$

where  $\varepsilon_{ij}$  represents the strain tensor. From the strained lattice basis vectors, the strained reciprocal lattice vectors can be obtained, which are used for the diagonalization of the Hamiltonian matrix and the calculation of the normalizing volume of the strained unit cell, i.e.,

$$\Omega'_0 = \Omega_0(1 + \varepsilon_{xx} + \varepsilon_{yy} + \varepsilon_{zz}). \quad (2)$$

- 2) Since the local pseudopotential form factors enter the calculation at the strained reciprocal lattice vectors, an interpolation of the pseudopotential is required. Several expressions have been proposed [12], [13]. We follow [12] using  $k_F = 1.66(2\pi/a_0)$  for the Fermi wave vector.
- 3) Generally, the macroscopic strain is not sufficient to determine the absolute positions of the two atoms in the bulk primitive unit cell. An additional displacement has to be accounted for, which is frequently quantified using the internal strain parameter  $\xi$ . In the case of general strain, the displacement of the central atom with respect to the four vertex atoms that span the unit tetrahedron in the diamond structure is calculated in the following manner: First, the positions of the vertex atoms and the central atom are derived from the macroscopic strain. Afterward, the center of the four vertex atoms is determined, which does not necessarily coincide with the position of the central atom. As a consequence, the central atom moves toward the center of the four vertex atoms to minimize the nearest neighbor central force energy of the system. How-

ever, opposing this reduction of energy is the increase of the nearest neighbor noncentral force energy and the far-neighbor energy [14]. The actual displacement of the central atom is thus frequently modeled in terms of an internal displacement factor  $\xi$ . For  $\xi = 0$ , the central atom retains its position determined from the macroscopic strain only; for  $\xi = 1$ , the central atom moves to the center of the four vertex atoms, so all four bonds are of the same length. We used a value of  $\xi = 0.53$ , which has been obtained theoretically [15].

- 4) Strain-induced symmetry breaking increases the size of the irreducible wedge, which is required for band-structure calculations [16].

### B. Shear Strain Effects

The degeneracy of the two lowest conduction bands  $\Delta_1$  and  $\Delta_2'$  at the zone-boundary  $X$  points is a result of the crystal symmetry of Si and can be lifted by reducing the symmetry by applying strain. Whenever the strain tensor in the principal crystal system contains nonvanishing shear elements (e.g., as a result of stress along  $\langle 110 \rangle$ ), the strained lattice belongs to an orthorhombic crystal system, and the degeneracy is lifted. From the  $\mathbf{k} \cdot \mathbf{p}$  theory including terms of third order, Bir and Pikus found that by lifting the degeneracy at a zone-boundary  $X$  point, a comparatively large change in the energy dispersion of the conduction-band minimum located close to this  $X$  point is induced [17]. This effect was verified experimentally by Hensel *et al.* [18], who measured the change in effective mass in Si stressed along  $\langle 110 \rangle$ .

In unstrained Si, the constant energy surfaces of the six conduction-band valleys ( $\Delta_6$  valleys) have a prolate ellipsoidal shape, where the semiaxes are characterized by  $m_l$  and  $m_t$ , denoting the longitudinal and transverse electron masses, respectively. The minima of the three valley pairs are located along the three equivalent  $\langle 100 \rangle$  directions and have the same band-edge energies. A nonvanishing shear component  $\varepsilon_{xy}$  in the strain tensor affects the energy dispersion of the lowest conduction band in three ways.

- 1) The band-edge energy of the valley pair ( $\Delta_2$  valleys) oriented along the  $[001]$  direction moves down with respect to the four  $\Delta_4$  valleys oriented along  $[100]$  and  $[010]$ .
- 2) The effective mass of the  $\Delta_2$  valleys changes; at small shear strain, the constant energy surfaces take the form of scalene ellipsoids characterized by three masses, i.e.,  $m_{l,[001]}$ ,  $m_{t,[110]}$ , and  $m_{t,[\bar{1}10]}$ .
- 3) The position of the  $\Delta_2$  valley minima moves toward the zone-boundary  $X$  points,  $\mathbf{k}_X = 2\pi/a_0(0, 0, \pm 1)$ .

Using a degenerate  $\mathbf{k} \cdot \mathbf{p}$  theory at the zone-boundary  $X$  point, neglecting spin-orbit and nonlocal effects, analytical expressions characterizing the shape of the strained conduction-band minima at  $\mathbf{k}_0 = 2\pi/a_0(0, 0, 0.85)$  can be derived [17], [18]. From these formulas, we derived the energy shift between the  $\Delta_2$  valleys with respect to the  $\Delta_4$  valleys, i.e.,

$$\Delta E_{\text{shear}} = \begin{cases} -\varepsilon_{xy}^2 \Delta / 4\kappa^2, & |\varepsilon_{xy}| < \kappa \\ -(2|\varepsilon_{xy}/\kappa| - 1)\Delta/4, & |\varepsilon_{xy}| > \kappa \end{cases} \quad (3)$$

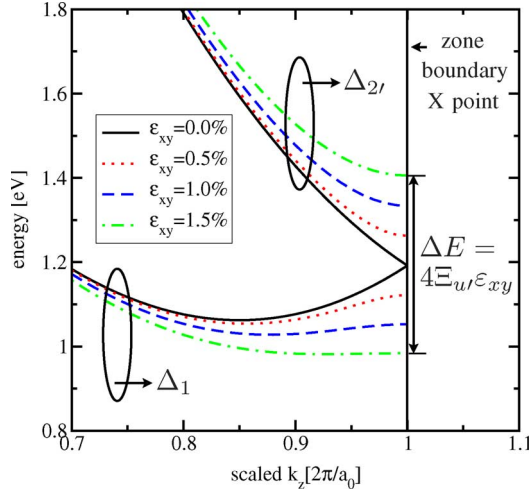


Fig. 1. EPM calculations of the two lowest conduction bands of Si near the zone-boundary  $X$  point,  $\vec{k} = (2\pi/a_0)(0, 0, 1)$ , in the absence of shear strain (solid curves) and with  $\varepsilon_{xy}$  applied (dotted, dashed, and dash-dotted curves).

Here, a dimensionless parameter  $\kappa$  has been introduced. It is given by  $\kappa = \Delta/(4\Xi_{u'})$ , where  $\Delta$  is the band separation between the two lowest conduction bands at the conduction-band edge of the unstrained lattice, and  $\Xi_{u'}$  is the deformation potential responsible for the band splitting of the two lowest conduction bands at the zone boundary [18], i.e.,

$$(E_{\Delta_1} - E_{\Delta_2})|_{X_{[001]}} = 4\Xi_{u'}\varepsilon_{xy}. \quad (4)$$

For arbitrary strain conditions, the energy shift from axial strain  $\Delta E_{\text{axial}}$  has to be added to the energy shift induced by shear strain to calculate the total energy shift of the  $\Delta_2$  valley pair along [001], i.e.,

$$\Delta E_{\text{axial}} = \Xi_d(\varepsilon_{xx} + \varepsilon_{yy} + \varepsilon_{zz}) + \Xi_u\varepsilon_{zz} \quad (5)$$

$$\Delta E_{\text{tot}} = \Delta E_{\text{axial}} + \Delta E_{\text{shear}}. \quad (6)$$

The energy shift from axial strain is determined by the two deformation potentials  $\Xi_u$  and  $\Xi_d$  [19], [20].

The effective masses of the valley pair along the [001] direction are given by

$$m_{l,[001]}(\varepsilon_{xy})/m_l = \begin{cases} (1 - \varepsilon_{xy}^2/\kappa^2)^{-1}, & |\varepsilon_{xy}| < \kappa \\ (1 - \kappa/|\varepsilon_{xy}|)^{-1}, & |\varepsilon_{xy}| > \kappa \end{cases} \quad (7)$$

$$m_{t,[110]}(\varepsilon_{xy})/m_t = \begin{cases} (1 - \eta\varepsilon_{xy}/\kappa)^{-1}, & |\varepsilon_{xy}| < \kappa \\ (1 - \text{sgn}(\varepsilon_{xy})\eta)^{-1}, & |\varepsilon_{xy}| > \kappa \end{cases} \quad (8)$$

$$m_{t,[\bar{1}10]}(\varepsilon_{xy})/m_t = \begin{cases} (1 + \eta\varepsilon_{xy}/\kappa)^{-1}, & |\varepsilon_{xy}| < \kappa \\ (1 + \text{sgn}(\varepsilon_{xy})\eta)^{-1}, & |\varepsilon_{xy}| > \kappa. \end{cases} \quad (9)$$

Here,  $\text{sgn}$  denotes the signum function. It should be noted that a unique expression for the parameter  $\eta$  can be derived using the  $\mathbf{k} \cdot \mathbf{p}$  theory [21].

### C. EPM Results

The strain-induced lifting of the degeneracy of the  $\Delta_1$  and  $\Delta_2$  conduction bands is shown in Fig. 1. The three effects

TABLE II  
RESULTS FROM Si EPM CALCULATIONS

parameter	EPM result	parameter	EPM result
$\Xi_u$ (eV)	9.29	$m_l$ ( $m_0$ )	0.916
$\Xi_d$ (eV)	1.1	$m_t$ ( $m_0$ )	0.194
$\Xi_{u'}$ (eV)	7.0	$\kappa$	0.0189
$\Delta$ (eV)	0.53	$\eta$	-0.809

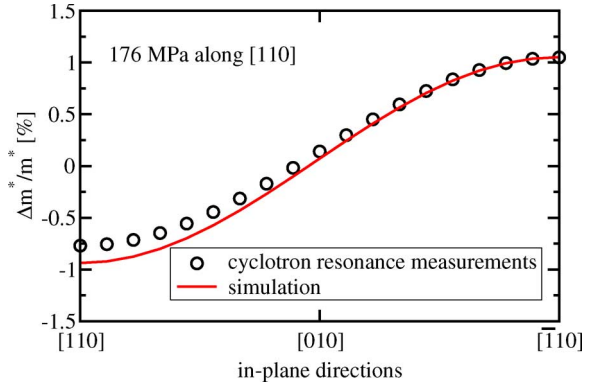


Fig. 2. Calculated anisotropy of the cyclotron resonance effective mass  $m^* = \sqrt{m_t m_l}$  of the (001) ellipsoid for 176-MPa tensile stress along [110] as compared to measurements [18]. The effective mass change in the (001) plane is consistent with experimental data.

induced by shear strain  $\varepsilon_{xy}$  on the  $\Delta_1$  band minima along [001] can be clearly observed: 1) the change of the band-edge energy; 2) the change of the effective masses; and 3) the change of the position of the band minimum. Calculations indicate that  $\varepsilon_{xy}$  does not change the conduction-band valleys along [100] and [010], which is consistent with theoretical arguments from symmetry considerations.

The parameters required in the analytical expressions (3)–(9) were extracted from EPM calculations and are summarized in Table II. In agreement with [12], a value of 9.29 eV was extracted for  $\Xi_u$ . The dilatation deformation potential  $\Xi_d$ , which cannot directly be determined from EPM calculations, was set to 1.1 eV [6]. The value for the shear deformation potential  $\Xi_{u'} = 7.0$  eV lies between the experimental value of 5.7 eV [18] and the theoretical value of 7.8 eV [22]. The band separation  $\Delta$  at the conduction-band edge is found to be 0.53 eV, yielding a value of 0.0189 for the parameter  $\kappa$  entering the analytical expressions (3) and (7)–(9).

The effective masses were extracted from EPM calculations by computing the curvature of the minima of the first conduction band. In unstrained Si, the obtained values, i.e.,  $m_l = 0.916 m_0$  and  $m_t = 0.194 m_0$ , are in close agreement to experimental data. The calculated change of the effective mass induced by shear strain has been compared to values extracted from cyclotron resonance measurements. Good agreement is achieved, as can be seen in Fig. 2. Finally, we evaluated the parameter  $\eta = -0.809$  from band-structure calculations.

The splitting between the  $\Delta_2$  and  $\Delta_4$  conduction-band valleys induced by shear strain  $\varepsilon_{xy}$  is shown in Fig. 3, where results from EPM calculations are compared to the analytical expression (3). Note that for both positive and negative shear strain, the  $\Delta_2$  valley pair moves down in energy with respect to the  $\Delta_4$  valleys.

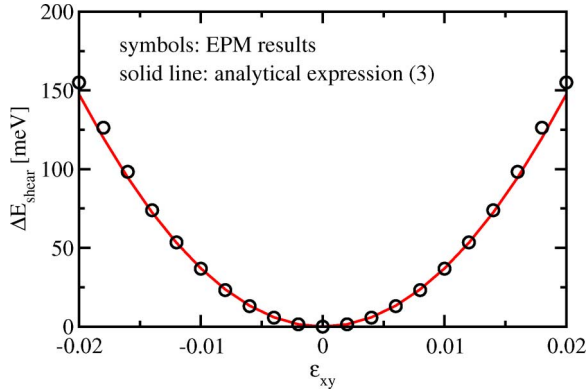


Fig. 3. Shift of the minima of the  $\Delta_{[100]}$  and  $\Delta_{[010]}$  valleys with respect to the  $\Delta_{[001]}$  valleys induced by shear strain  $\varepsilon_{xy}$ . Comparison with analytical result from (3).

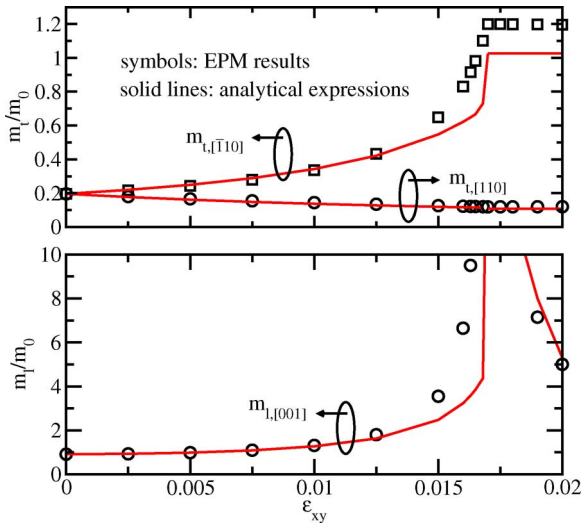


Fig. 4. Comparison of EPM calculations for the effective masses along the directions [001], [110], and  $[\bar{1}10]$  with analytical expressions (7)–(9).

In Fig. 4, the effective mass dependence on shear strain  $\varepsilon_{xy}$  extracted directly from EPM calculations is compared to the analytical expressions. Good agreement can be observed for  $\varepsilon_{xy} < 1.5\%$ ; for larger values of shear strain, the change of the effective masses as obtained from the  $\mathbf{k} \cdot \mathbf{p}$  theory is smaller than that from EPM calculations.

Furthermore, it was found that uniaxial tensile stress along  $\langle 100 \rangle$  does not significantly change the transverse masses in any of the six conduction-band valleys, which is consistent with the theoretical calculations of Rieger and Vogl [12] and Uchida *et al.* [23].

### III. SIMULATION OF ELECTRON MOBILITY

Electron mobility was calculated numerically by solving the semiclassical Boltzmann equation using an MC method. For this purpose, the simulator Vienna Monte Carlo (VMC) [24] was developed, offering simulation algorithms for both bulk semiconductors and 1-D devices with models based either on both analytical bands (ABMC) or the full-band structure (FBMC). VMC provides a comprehensive set of scattering models, including phonon scattering, ionized impurity scat-

TABLE III  
MODES, COUPLING CONSTANTS, PHONON ENERGIES, AND SELECTION RULE OF INELASTIC PHONON SCATTERING

Mode	$\Delta$ [MeV/cm]	$\hbar\omega$ [meV]	selection rule
Transversal Acoustic	47.2	12.1	f
Longitudinal Acoustic	75.5	18.5	f
Longitudinal Optical	1042.0	62.0	f
Transversal Acoustic	34.8	19.0	g
Longitudinal Acoustic	232.0	47.4	g
Transversal Optical	232.0	58.6	g

tering, alloy scattering, and impact ionization. Additionally, the effective mobility in Si inversion layers can be calculated using ellipsoidal nonparabolic subbands. For the calculation of the 2-D subband energies and envelope wave functions, the Schrödinger and Poisson equations are solved self-consistently using VSP [25].

For the subband transport calculations, the Si conduction band was approximated by three nonparabolic ellipsoidal valley pairs using the masses that were extracted from the EPM calculations and a nonparabolicity coefficient  $\alpha$  of  $0.5 \text{ eV}^{-1}$ . The strain effects are modeled using the analytical expressions (3) and (7)–(9); thus, both the effective mass change in the  $\Delta_2$  valley and the additional valley shift are taken into account.

#### A. Bulk Scattering Models

A phonon scattering model that is based on the well-accepted bulk phonon spectrum of Jacoboni and Reggiani [26] was used. The model takes into account long-wavelength acoustic phonons causing intravalley transitions and three f-type and g-type phonons for intervalley transitions. Intravalley scattering from acoustic phonons is treated as an elastic process using the value of 9.0 eV for the acoustic deformation potential. For intervalley phonon scattering, we adjusted the original values for the coupling constants given in [26], as discussed in [27], to achieve a bulk mobility enhancement factor of 70% in biaxially strained-Si layers.

For full-band simulations, phonon scattering models with constant matrix elements are used [28]. In this formulation, the scattering rates are proportional to the density of states calculated from the band structure. The coupling constants for acoustic and optical intervalley phonons, as well as the phonon energies, are given in Table III.

#### B. Inversion-Layer Scattering Models

In the Si inversion layer, phonon scattering and surface roughness scattering as the dominant sources of scattering at large inversion-layer concentrations are accounted for, whereas impurity scattering producing deviations from the universal mobility at low inversion-layer concentrations is neglected. Degeneracy effects are included, as the 2-D electron gas (2DEG) is highly degenerate at high inversion-layer concentrations [29].

The bulk phonon scattering model has been adapted for the 2DEG following the treatment of Price [30]. In the 2DEG, scattering with long-wavelength acoustic phonons causes

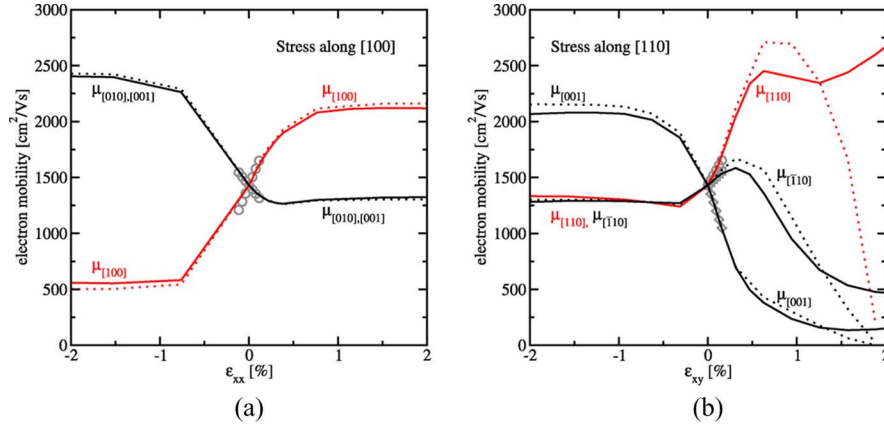


Fig. 5. Simulated bulk mobility of intrinsic Si as a function of strain for stress direction (a) [100] and (b) [110]. Mobility is plotted along the stress direction and along two orthogonal directions from (solid lines) FBMC and (dotted lines) ABMC. Symbols indicate the change of mobility calculated using the piezoresistance coefficients [2].

intrasubband and intersubband transitions within the same subband ladder. The three f-type and g-type phonons can additionally cause transitions to different subband ladders [31]. The value of the acoustic deformation potential was adjusted to 14.8 eV. The surface roughness scattering rate was modeled according to Esseni [32], who adapted the original approach of Ando *et al.* [33] for scattering at two interfaces. The step height  $\Delta$  and the correlation length  $L$  characterizing the interface roughness were chosen to be 0.4 and 1.3 nm, respectively. Screening was accounted for using a numerically calculated expression of the 2-D static dielectric function [31].

### C. Bulk Mobility Results

Comparing the simulation results from ABMC with FBMC allows the following: 1) a direct interpretation of the FBMC results and 2) the extraction of the limits of validity of the analytical band model. In Fig. 5, we compare the simulation results for the electron mobility of strained-Si obtained with FBMC and ABMC for the stress directions [100] and [110]. Mobility is plotted in three orthogonal directions, one being parallel and two being perpendicular to stress.

In Fig. 5(a), the simulation results from ABMC and FBMC for stress along [100] are compared, and good agreement can be observed. The resulting mobility is anisotropic in the (001) plane ( $\mu_{[100]} \neq \mu_{[010]}$ ) and can solely be explained as a result of strain-induced X-valley shifts. Mobility saturates at approximately 1% strain regardless of the sign of strain. The saturated mobility values are larger for compressive strain since for this type of strain, four X-valleys are being depopulated, whereas for tensile strain, only two valleys are being depopulated. Thus, the larger amount of intervalley scattering and the larger transport mass of the two populated valley pairs reduce the mobility enhancement for tensile stress.

In Fig. 5(b), the simulation results are shown for stress along [110]. At compressive stress (negative  $\epsilon_{xy}$ ), four valleys move down in energy, yielding a decreased mobility in the (001) plane and mobility enhancement along [001]. However, if tensile stress is applied along [110], the strain-induced mobility enhancement is remarkably different from the other cases:

Mobilities along the three directions, i.e., [110],  $[\bar{1}10]$ , and [001], are different from each other, with the largest mobility enhancement in the [110] direction. Furthermore, no clear in-plane mobility saturation is observed as  $\epsilon_{xy}$  increases. The reason for the unsimilar mobility enhancement at the [110] tensile stress is that, for this stress, the valley pair along [001] is primarily populated. As shown in Section II-B, this valley pair experiences a pronounced deformation as a function of shear strain  $\epsilon_{xy}$ .

In our ABMC simulation, this deformation was accounted for by using expressions (3) and (7)–(9) to model the changing shape of the conduction-band valley as a function of shear strain. It can be seen that the simulation results from ABMC qualitatively agree with those from FBMC up to 0.5% shear strain. At larger strain levels, the band deformation is very pronounced that an energy-band description in terms of an effective mass is no longer accurate, and FBMC has to be used to calculate the low-field mobility. It should be noted that an even better agreement between ABMC and FBMC could be obtained if the strain effect on the nonparabolicity coefficient  $\alpha$  was included in the analytical band model.

The simulated mobility enhancement for stress along [100] and [110] was checked with predictions from a model based on the linear piezoresistance coefficients [2]. Good agreement is found for both stress directions at small stress ( $< 200$  MPa) where the model is valid (compare with Fig. 5). Models solely based on strain-induced intervalley electron transfer [19] fail to explain the origin of the nonvanishing shear piezoresistance coefficient  $\pi_{44} = -13.6 \cdot 10^{-11} \text{ Pa}^{-1}$ ; hence, these models are not capable of reproducing the anisotropy of electron mobility in uniaxially stressed channels with the [110] channel direction [34], [35].

### D. Channel Mobility Results

Depending on the substrate orientation, the  $\Delta_6$  valleys split into up to three different subband ladders. On substrates with (001) standard orientation two subband ladders arise, a two-fold degenerate ladder (unprimed ladder) with spherical energy dispersion, and a four-fold degenerate ladder (primed ladder)

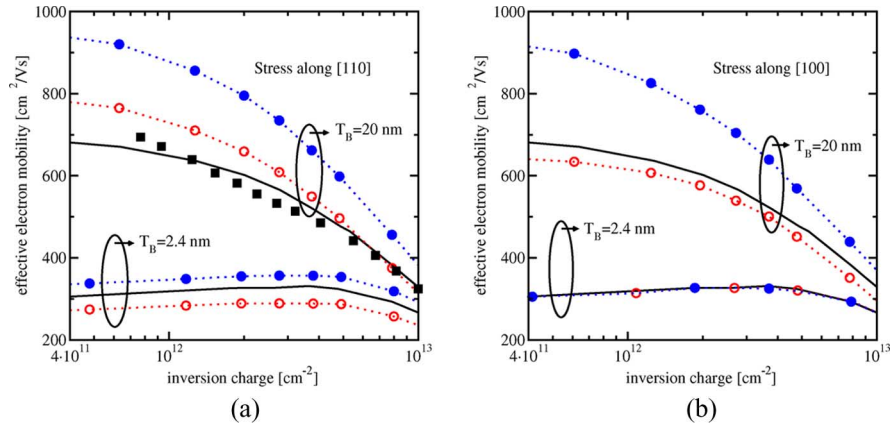


Fig. 6. Simulated effective mobility for substrate orientation (001) of (solid lines) unstrained and (dashed lines) 1-GPa stressed Si for two body thicknesses. The mobility components are plotted (closed symbols) parallel and (open symbols) perpendicular to the stress direction (a) [110] and (b) [100]. Closed squares show experimental data for unstrained silicon-on-insulator with  $T_B = 22$  nm from [38].

with elliptical subbands. Compared to other substrate orientations, the (001) orientation intrinsically yields the largest effective mobility for electrons, which is isotropic in the plane of transport [36], [37].

In this paper, the channel mobility enhancement for strained (001)-oriented substrate is investigated for two cases: stress and channel both parallel to the [110] direction and to the [100] direction. Additionally, the impact of the Si body thickness on the mobility enhancement is highlighted.

In Fig. 6(a), the mobility parallel and perpendicular to the channel direction [110] under 1-GPa stress along [110] is compared to the unstrained mobility at two Si body thicknesses. At relatively large body thicknesses ( $T_B > 20$  nm), tensile stress along [110] has two beneficial effects on the [110] mobility: The splitting between the unprimed and primed ladders is increased, and the transport mass in stress direction is reduced with respect to the unstrained case. From these two effects, one can understand the mobility enhancement parallel to the stress direction at all inversion-layer densities. In  $\bar{[110]}$ , perpendicular to stress, the effective mass is increased, leading to a smaller mobility enhancement in this direction at small inversion-layer concentration, which further diminishes at large inversion-layer concentrations.

For very small body thickness ( $T_B < 5$  nm), the energetical separation between the subband ladders is higher due to strong quantum confinement. Thus, the stress-induced valley shifts have a negligible effect on the mobility, and the larger (smaller) mobility parallel (perpendicular) to stress results from the effective mass change only and is found to be in good agreement with experimental data [23], [37].

In Fig. 6(b), the effect of uniaxial stress on the mobility with channel direction and stress direction parallel to [100] is shown. Stress along [100] lifts the degeneracy of the fourfold (primed) ladder; thus, three subband ladders arise. Since no effective mass change occurs,  $\Delta\mu_{\text{eff}}$  occurring at large  $T_B$  is a result of subband ladder repopulation only. As the body thickness is decreased, the subband separation increases, and thus, the population of the higher subband ladders inevitably decreases, such that strain cannot further decrease the population. Therefore, the initial mobility enhancement parallel to stress seen at large  $T_B = 20$  nm vanishes at  $T_B = 2.4$  nm.

#### IV. SUMMARY AND CONCLUSION

The effect of general strain on the band structure of Si was systematically investigated by means of EPM band-structure calculations. A pronounced effect of shear strain on the conduction-band shape has been observed and was quantified in terms of the following: 1) an effective mass change and 2) a shear-strain-induced valley splitting. Analytical expressions for both effects have been derived using the  $\mathbf{k} \cdot \mathbf{p}$  theory. The band structure was used in FBMC simulations to analyze the effect of strain on the electron mobility. MC simulations using an analytical description of the electron bands were shown to be valid in a certain range of shear strain ( $< \pm 0.5\%$ ). At larger shear strain, however, the band deformation is very pronounced that full-band modeling is required. Using MC simulations and a rigorous modeling of the strain effect on the electronic band structure, the limits of the linear piezoresistance model can be determined to calculate the electron mobility under general strain. In Si inversion layers on (001)-oriented substrate with small body thickness, the effective mass change by shear strain is the only mechanism able to enhance the electron mobility.

#### REFERENCES

- [1] H. H. Hall, J. Bardeen, and G. L. Pearson, "The effects of pressure and temperature on the resistance of  $p-n$  junctions in germanium," *Phys. Rev.*, vol. 84, no. 1, pp. 129–132, Oct. 1951.
- [2] C. S. Smith, "Piezoresistance effect in germanium and silicon," *Phys. Rev.*, vol. 94, no. 1, pp. 42–49, Apr. 1954.
- [3] E. Fitzgerald, Y. Xie, M. Green, D. Brasen, A. Kortan, J. Michel, Y. Mii, and B. Weir, "Totally relaxed  $\text{Ge}_x\text{Si}_{1-x}$  layers with low threading dislocation densities grown on Si substrates," *J. Appl. Phys.*, vol. 59, no. 7, pp. 811–813, Aug. 1991.
- [4] J. Welser, J. Hoyt, and J. Gibbons, "NMOS and PMOS transistors fabricated in strained silicon/relaxed silicon-germanium structures," in *IEDM Tech. Dig.*, 1992, pp. 1000–1002.
- [5] J. Welser, J. Hoyt, and J. Gibbons, "Electron mobility enhancement in strained-Si n-type metal-oxide-semiconductor field-effect transistors," *IEEE Electron Device Lett.*, vol. 15, no. 3, pp. 100–102, Mar. 1994.
- [6] M. V. Fischetti and S. E. Laux, "Band structure, deformation potentials, and carrier mobility in strained Si, Ge, and SiGe alloys," *J. Appl. Phys.*, vol. 80, no. 4, pp. 2234–2252, Aug. 1996.
- [7] F. M. Butler, P. Graf, S. Keith, and B. Meinerzhagen, "Full band Monte Carlo investigation of electron transport in strained Si grown on  $\text{Si}_{1-x}\text{Ge}_x$  substrates," *Appl. Phys. Lett.*, vol. 70, no. 16, pp. 2144–2146, Apr. 1997.

- [8] C. Jungemann and B. Meinerzhagen, "MC simulation of strained Si/SiGe devices," in *Proc. 33rd Eur. Solid-State Device Res. Conf.*, 2003, pp. 9–14.
- [9] J. R. Chelikowsky and M. L. Cohen, "Nonlocal pseudopotential calculations for the electronic structure of eleven diamond and zincblende semiconductors," *Phys. Rev. B, Condens. Matter*, vol. 14, no. 2, pp. 556–582, Jul. 1976.
- [10] P. Yu and M. Cardona, *Fundamentals of Semiconductors*. New York: Springer-Verlag, 2003.
- [11] C. G. Van de Walle and R. M. Martin, "Theoretical calculations of heterojunction discontinuities in the Si/Ge system," *Phys. Rev. B, Condens. Matter*, vol. 34, no. 8, pp. 5621–5634, Oct. 1986.
- [12] M. M. Rieger and P. Vogl, "Electronic-band parameters in strained  $\text{Si}_{1-x}\text{Ge}_x$  alloys on  $\text{Si}_{1-y}\text{Ge}_y$  substrates," *Phys. Rev. B, Condens. Matter*, vol. 48, no. 19, pp. 14 276–14 287, Nov. 1993.
- [13] P. Friedel, M. S. Hybertsen, and M. Schlüter, "Local empirical pseudopotential approach to the optical properties of Si/Ge superlattices," *Phys. Rev. B, Condens. Matter*, vol. 39, no. 11, pp. 7974–7977, Apr. 1989.
- [14] L. Kleinman, "Deformation potentials in silicon. I. Uniaxial strain," *Phys. Rev.*, vol. 128, no. 6, pp. 2614–2621, Dec. 1962.
- [15] O. Nielsen and R. Martin, "Stresses in semiconductors: Ab initio calculations on Si, Ge, and GaAs," *Phys. Rev. B, Condens. Matter*, vol. 32, no. 6, pp. 3792–3805, Sep. 1985.
- [16] E. Ungersboeck, S. Dhar, G. Karlowatz, H. Kosina, and S. Selberherr, "Physical modeling of electron mobility enhancement for arbitrarily strained silicon," in *Proc. 11th Int. Workshop Comput. Electron. Book Abstracts*, 2006, pp. 141–142.
- [17] G. L. Bir and G. E. Pikus, *Symmetry and Strain Induced Effects in Semiconductors*. New York: Wiley, 1974.
- [18] J. C. Hensel, H. Hasegawa, and M. Nakayama, "Cyclotron resonance in uniaxially stressed silicon. II. Nature of the covalent bond," *Phys. Rev.*, vol. 138, no. 1A, pp. A225–A238, Apr. 1965.
- [19] C. Herring and E. Vogt, "Transport and deformation-potential theory for many-valley semiconductors with anisotropic scattering," *Phys. Rev.*, vol. 101, no. 3, pp. 944–961, Feb. 1956.
- [20] I. Balslev, "Influence of uniaxial stress on the indirect absorption edge in silicon and germanium," *Phys. Rev.*, vol. 143, no. 3, pp. 636–647, Mar. 1966.
- [21] E. Ungersboeck, "Advanced modeling of strained CMOS technology," Ph.D. dissertation, Vienna Tech. Univ., Vienna, Austria, 2007. [Online]. Available: <http://www.iue.tuwien.ac.at/phd/ungersboeck/>
- [22] I. Goroff and L. Kleinman, "Deformation potentials in silicon. III. Effects of a general strain on conduction and valence levels," *Phys. Rev.*, vol. 132, no. 3, pp. 1080–1084, Nov. 1963.
- [23] K. Uchida, T. Krishnamohan, K. Saraswat, and Y. Nishi, "Physical mechanisms of electron mobility enhancement in uniaxial stressed MOSFETs and impact of uniaxial stress engineering in ballistic regime," in *IEDM Tech. Dig.*, 2005, pp. 135–138.
- [24] *VMC2.0, Vienna Monte Carlo 2.0 User's Guide*, Institut für Mikroelektronik, Technische Universität Wien, Vienna, Austria, 2006. [Online]. Available: <http://www.iue.tuwien.ac.at/software>
- [25] M. Karner, A. Gehring, S. Holzer, M. Pourfath, M. Wagner, H. Kosina, T. Grasser, and S. Selberherr, "VSP—A multi-purpose Schrödinger-Poisson solver for TCAD applications," in *Proc. 11th Int. Workshop Comput. Electron. Book Abstracts*, 2006, pp. 255–256.
- [26] C. Jacoboni and L. Reggiani, "The Monte Carlo method for the solution of charge transport in semiconductors with applications to covalent materials," *Rev. Mod. Phys.*, vol. 55, no. 3, pp. 645–705, Jul. 1983.
- [27] S. Dhar, H. Kosina, G. Karlowatz, E. Ungersboeck, T. Grasser, and S. Selberherr, "High-field electron mobility model for strained-silicon devices," *IEEE Trans. Electron Devices*, vol. 53, no. 12, pp. 3054–3062, Dec. 2006.
- [28] C. Jungemann and B. Meinerzhagen, *Hierarchical Device Simulation: The Monte Carlo Perspective*, ser. Computational Microelectronics. New York: Springer-Verlag, 2003.
- [29] E. Ungersboeck and H. Kosina, "Monte Carlo study of electron transport in strained silicon inversion layers," *J. Comput. Electron.*, vol. 5, no. 2/3, pp. 79–83, Jul. 2006.
- [30] P. J. Price, "Two-dimensional electron transport in semiconductor layers. I. Phonon scattering," *Ann. Phys.*, vol. 133, no. 2, pp. 217–239, May 1981.
- [31] C. Jungemann, A. Edmunds, and W. Engl, "Simulation of linear and nonlinear electron transport in homogeneous silicon inversion layers," *Solid State Electron.*, vol. 36, no. 11, pp. 1529–1540, Nov. 1993.
- [32] D. Esseni, "On the modeling of surface roughness limited mobility in SOI MOSFETs and its correlation to the transistor effective field," *IEEE Trans. Electron Devices*, vol. 51, no. 3, pp. 394–401, Mar. 2004.
- [33] T. Ando, A. Fowler, and F. Stern, "Electronic properties of two-dimensional systems," *Rev. Mod. Phys.*, vol. 54, no. 2, pp. 437–672, Apr. 1982.
- [34] T. Maruyama, S. Zaima, Y. Koide, Y. Kanda, and Y. Yasuda, "Anisotropy of piezoresistance in n-channel inversion layers of metal-oxide-semiconductor transistors on (001)Si," *J. Appl. Phys.*, vol. 68, no. 11, pp. 5687–5691, Dec. 1990.
- [35] Y. Kanda and K. Suzuki, "Origin of the shear piezoresistance coefficient  $\pi_{44}$  of n-type silicon," *Phys. Rev. B, Condens. Matter*, vol. 43, no. 8, pp. 6754–6756, Mar. 1991.
- [36] G. Tsutsui, M. Saitoh, T. Saraya, T. Nagumo, and T. Hiramotyo, "Mobility enhancement due to volume inversion in (110)-oriented ultra-thin body double-gate nMOSFETs with body thickness less than 5 nm," in *IEDM Tech. Dig.*, 2005, pp. 747–750.
- [37] H. Irie, K. Kita, K. Kyuno, and A. Toriumi, "In-plane mobility anisotropy and universality under uni-axial strains in n- and p-MOS inversion layers on (100), (110), and (111) Si," in *IEDM Tech. Dig.*, 2004, pp. 225–228.
- [38] K. Uchida, J. Koga, and S. Takagi, "Experimental study on carrier transport mechanisms in double- and single-gate ultrathin-body MOSFETs—Coulomb scattering, volume inversion, and  $\delta$ TSOI-induced scattering," in *IEDM Tech. Dig.*, 2003, pp. 805–808.



**Enzo Ungersboeck** was born in Vienna, Austria, in 1977. He received the Dipl.Ing. degree in physics from the Technische Universität Wien, Vienna, in 2002. He is currently working toward the Ph.D. degree in the Institut für Mikroelektronik, Technische Universität Wien.

He held a visiting research position with Samsung Advanced Institute of Technology, Seoul, South Korea, in the summer of 2003. His scientific interests include Monte Carlo simulation, band-structure calculations, simulation of carbon nanotubes, and quantum-mechanical confinement in submicrometer MOSFETs.



**Siddhartha Dhar** (S'06) was born in New Delhi, India, in 1979. He received the B.E. degree in electrical engineering from the Delhi College of Engineering, Delhi, India, in 2001 and the M.Sc. degree in microelectronics and microsystems from the Technical University of Hamburg-Harburg, Hamburg, Germany, in 2003. He is currently working toward the Ph.D. degree in the Institut für Mikroelektronik, Technische Universität Wien, Vienna, Austria.

His research interests include device modeling and simulation of strained-silicon CMOS transistors and circuit-level simulation in general.



**Gerhard Karlowatz** was born in Mödling, Austria, in 1972. He received the Dipl.Ing. degree in physics from the Technische Universität Wien, Vienna, Austria, in 2003. He is currently working toward the Ph.D. degree in the Institut für Mikroelektronik, Technische Universität Wien.

His scientific interests include Monte Carlo simulation and modeling of optical devices.



**Viktor Sverdlov** received the M.Sc. and Ph.D. degrees in physics from the State University of St. Petersburg, St. Petersburg, Russia, in 1985 and 1989, respectively.

From 1989 to 1999, he was a Staff Research Scientist with the V. A. Fock Institute of Physics, St. Petersburg State University. During this time, he held visiting research positions at several European research centers and universities, namely: Abdus Salam International Centre for Theoretical Physics, Trieste, Italy, in 1993; the University of Geneva, Geneva, Switzerland, in 1993–1994; the University of Oulu, Oulu, Finland, in 1995; Helsinki University of Technology, Helsinki, Finland, in 1996–1998; Free University of Berlin, Berlin, Germany, in 1997; and Nordic Institute for Theoretical Physics, Copenhagen, Denmark, in 1998. In 1999, he became a Staff Research Scientist with the State University of New York at Stony Brook. He joined the Institut für Mikroelektronik, Technische Universität Wien, Vienna, Austria, in 2004. His scientific interests include device simulation, computational physics, solid-state physics, and nanoelectronics.



**Hans Kosina** (S'89–M'93) received the Dipl.Ing. degree in electrical engineering, the Ph.D. degree, and the “Venia docendi” degree in microelectronics from the Technische Universität Wien, Vienna, Austria, in 1987, 1992, and 1998, respectively.

He was with the Institute of Flexible Automation, Technische Universität Wien, for one year and then joined the Institut für Mikroelektronik, Technische Universität Wien, where he is currently an Associate Professor. In the summer of 1993, he was a Visiting Scientist with Motorola Inc., Austin, TX, and in the summer of 1999, he was a Visiting Faculty with Intel Corporation, Santa Clara, CA. His current research interests include device modeling of semiconductor devices, nanoelectronic devices, organic semiconductors and optoelectronic devices, development of novel Monte Carlo algorithms for classical and quantum transport problems, and computer-aided engineering in ULSI technology.

Dr. Kosina has been an Associate Editor of the IEEE TRANSACTIONS ON COMPUTER-AIDED DESIGN OF INTEGRATED CIRCUITS AND SYSTEMS since January 2004.



**Siegfried Selberherr** (M'79–SM'84–F'93) was born in Klosterneuburg, Austria, in 1955. He received the Dipl.Ing. degree in electrical engineering, the Ph.D. degree in technical sciences, and the “Venia docendi” degree in computer-aided design from the Technische Universität Wien, Vienna, Austria, in 1978, 1981, and 1984, respectively.

Since 1988, he has been a Chair Professor with the Institut für Mikroelektronik, Technische Universität Wien. From 1998 to 2005, he served as the Dean of the Fakultät für Elektrotechnik und Informationstechnik, Technische Universität Wien. His current research interests are modeling and simulation of problems for microelectronics engineering.